Measurements of ^{nat}Cd(γ, *x*) reaction cross sections and isomer ratio of ^{115m,g}Cd with the bremsstrahlung end-point energies of 50 and 60 MeV*

Muhammad Nadeem[1] Md. Shakilur Rahman[2] Muhammad Shahid[1] Guinyun Kim[1†]
Haladhara Naik[3] Nguyen Thi Hien[1]

[1]Department of Physics, Kyungpook National University, Daegu 41566, Korea
[2]Institute of Nuclear Science and Technology, Bangladesh Atomic Energy Commission, Savar, Dhaka, Bangladesh
[3]Radiochemistry Division, Bhabha Atomic Research Centre, Mumbai 400085, India

Abstract: The flux-weighted average cross sections of ^{nat}Cd(γ, *xn*)^{115g,m,111m,109,107,105,104}Cd and ^{nat}Cd(γ, *x*)^{113g,112,111g,110m}Ag reactions were measured at the bremsstrahlung end-point energies of 50 and 60 MeV. The activation and off-line γ-ray spectrometric technique was carried out using the 100 MeV electron linear accelerator at the Pohang Accelerator Laboratory, Korea. The ^{nat}Cd(γ, *xn*) reaction cross sections as a function of photon energy were theoretically calculated using the TALYS-1.95 and the EMPIRE-3.2 Malta codes. Then, the flux-weighted average cross sections were obtained from the theoretical values of mono-energetic photons. These values were compared with the flux-weighted values from the present study and were found to be in general agreement. The measured experimental reaction cross-sections and integral yields were described for cadmium and silver isotopes in the ^{nat}Cd(γ, *xn*)^{115g,m,111m,109,107,105,104}Cd and ^{nat}Cd(γ, *x*)^{113g,112,111g,110m}Ag reactions. The isomeric yield ratio (IR) of ^{115g,m}Cd in the ^{nat}Cd(γ, *xn*) reaction was determined for the two bremsstrahlung end-point energies. The measured isomeric yield ratios of ^{115g,m}Cd in the ^{nat}Cd(γ, *xn*) reaction were also compared with the theoretical values of the nuclear model codes and previously published literature data of the ^{116}Cd(γ, *n*) and ^{116}Cd(*n*, 2*n*) reactions. It was found that the IR value increases with increasing projectile energy, which demonstrates the characteristic of excitation energy. However, the higher IR value of ^{115g,m}Cd in the ^{116}Cd(*n*, 2*n*) reaction compared to that in the ^{116}Cd(γ, *n*) reaction indicates the role of compound nuclear spin alongside excitation energy.

Keywords: ^{nat}Cd(γ, *xn*) reaction cross sections, isomer yield ratio of ^{115g,m}Cd, off-line γ-ray spectrometric technique, TALYS-1.95, TENDL-2019, EMPIRE-3.2 Malta

DOI: 10.1088/1674-1137/ac256b

I. INTRODUCTION

Measurements of photon induced reaction cross-sections of natural cadmium are connected with different fields of science, such as the production of medically useful radioisotopes and yield measurements of long-lived radioactive products for radioactive waste handling and dose estimations. Cadmium isotopes are also used in nuclear technology as an important material to make bearings and alloys as well as for electroplating. Therefore, its activation can be used to estimate the radiation dose deposited inside materials for industrial or even medical purposes. In ^{nat}Cd, there are eight different isotopes [1]: ^{116}Cd (7.49%), ^{114}Cd (28.73%), ^{113}Cd (12.22%), ^{112}Cd (24.13%), ^{111}Cd (12.8%), ^{110}Cd (12.49%), ^{108}Cd (0.89%), and ^{106}Cd (1.25%). The proton induced reactions of ^{nat}Cd are good sources for the production of medically important indium radioisotopes [2]. The radioisotopes ^{111m}Cd and ^{111}In play a crucial role in time dependent perturbed angular correlation (TDPAC) studies for the investigation of material properties [3]. The radioisotope ^{109}Cd is frequently used for detector calibration due to its long half-life and high γ-ray abundance [4]. Cadmium isotopes are also used to enhance the coherence length and output power of HeCd metallic lasers [5]. Important radioactive isotopes of Cd can be produced from the photon-induced reactions of ^{nat}Cd. Similarly, the photon-induced reactions of ^{nat}Cd produce different radioisotopes of Ag. Among them, ^{110m}Ag is frequently used as a γ-ray reference source. The radioisotopes ^{111g}Ag and ^{110m}Ag are also medically important radioisotopes for radiotherapy and imaging purposes [2, 6].

Received 7 July 2021; Accepted 10 September 2021; Published online 19 October 2021

* Supported by the National Research Foundation of Korea (NRF) through a grant provided by the Ministry of Science and ICT (NRF-2017R1D1A1B03030484, NRF-2013M7A1A1075764, NRF-2018R1A6A1A06024970)

† E-mail: gnkim@knu.ac.kr

To maintain an optimal radioisotope production database, the addition of new, reliable experimental data is always important [7]. Previous studies were conducted in the giant dipole resonance (GDR) energy region for the production of ^{115m}Cd [8] and ^{111m}Cd [8, 9] using a γ-ray spectrometry technique; however, the [8, 9] results were higher than the estimated values. No further literature data have been found for any of the nuclides of interest, even in the GDR region. In a nuclear reaction, daughter products may have ground and meta-stable states with different nuclear spins. The ratio between the reaction cross sections of isomers with high spin (σ_H) and low spin (σ_L) is known as the isomeric yield ratio (σ_H/σ_L) [10]. There are few earlier experimental studies on the IR of ^{115m,g}Cd produced from the ^{116}Cd(γ, n)^{115m,g}Cd reaction in the giant dipole resonance region [11-14], based on mono-energetic photon beams. However, the measured IR of ^{g,m115}Cd in the ^{116}Cd(γ, n) reaction using bremsstrahlung endpoint energies of 50, 60, and 70 MeV is available in literature [15], and the IR at high neutron energies for the ^{116}Cd(n, 2n)^{115m,g}Cd reactions [16] is also cited.

Based on these data, in this study, well-established radiation activation and off-line γ-ray spectrometry were employed to determine the nuclear reaction cross-sections and integral yields of the ^{115g,m,111m,109,107,105,104}Cd and ^{113g,112,111g,110m}Ag radionuclides produced from ^{nat}Cd with the bremsstrahlung end-point energies of 50 and 60 MeV. The IR of ^{115m,g}Cd produced in the ^{nat}Cd(γ, n) reactions was also measured using the activation technique with these bremsstrahlung end-point energies. For comparison, the ^{nat}Cd(γ, xn)^{115g,m,111m,109,107,105,104}Cd and ^{nat}Cd(γ, pxn)^{113g,112,111g,110m}Ag reaction cross sections were also theoretically calculated by employing the computer codes TALYS-1.95 [17] and EMPIRE-3.2 Malta [18]. The IR values from the present study with the bremsstrahlung end-point energies of 50 and 60 MeV are compared with the calculated values [17, 18] as well as with the available literature data [11-15].

II. EXPERIMENTAL DETAILS

Pulsed electron beams from the 100 MeV electron LINAC installed at the Pohang Accelerator Laboratory (PAL), Korea, were utilized for bremsstrahlung production. The 50 and 60 MeV electron beams were individually bombarded, one energy beam at a time, onto a tungsten converter foil with a thickness of 0.1 mm and a size of 10 cm × 10 cm, which was placed at a distance of 18 cm from its exit window. Details regarding the bremsstrahlung production using the linear accelerator are described elsewhere [19, 20]. The high-purity (99.99%) natural cadmium and ^{197}Au metal foils were irradiated by bremsstrahlung radiation with end-point energies of 50 and 60 MeV. Two sets of 0.1 mm thick ^{nat}Cd foils with weights of 0.1782 and 0.1231 g and two sets of 0.1 mm thick ^{197}Au foils with weights of 0.2478 and 0.2668 g were placed in air at a distance of 12 cm from the W-target in a perpendicular direction to the electron beam. These targets were irradiated for 236 and 125 min with the bremsstrahlung radiation with end-point energies of 50 and 60 MeV, respectively. The average beam current during irradiation was 20-36 mA with a repetition rate of 15 Hz and a pulse width of 2 μs.

The samples irradiated by the bremsstrahlung radiation with end-point energies of 50 and 60 MeV were taken out after sufficient cooling time. The off-line γ-ray counting was performed using a pre-calibrated HPGe detector coupled with a PC-based 4K channel analyzer. The HPGe detector used for γ-ray counting is an Ortec detector from Canberra. The dead time of the detector during the γ-ray counting was kept below 2% by changing the distance between the detector and irradiated samples; this prevented pile up and coincidence-summing effects. The resolution of the HPGe detector was 1.8 keV at full-width at half width (FWHM) at the photopeak of 1332.5 keV γ-ray of ^{60}Co. The total detector efficiency was 20% at the 1332.5 keV γ-ray peak relative to a 7.62 cm × 7.62 cm NaI(Tl) detector. Typical γ-ray spectra of the reaction products produced from the ^{nat}Cd and ^{197}Au monitor samples irradiated with bremsstrahlung radiation with an end-point energy of 60 MeV are shown in Fig. 1(a-c). The produced radionuclides were identified based on the respective γ-ray energies and half-lives of the radioactive isotopes [21, 22], as presented in Table 1.

III. DATA ANALYSIS

A. Determination of photon flux

The photon fluxes ($\phi_{E_e}(E_\gamma)$) as a function of photon energy (E_γ) for the bremsstrahlung spectra with electron beam energies (E_e) of 50 and 60 MeV were simulated using the GEANT4 code [23] and are shown in Fig. 2. The integrated photon flux $\Phi(E_e)\left(=\int_{E_{th}}^{E_e}\phi_{E_e}(E_\gamma)\mathrm{d}E_\gamma\right)$ from the threshold to the electron beam energy was measured using the photo-peak activity of a 355.68 keV ($I\gamma$ =87%) γ-line of ^{196g}Au produced from the ^{197}Au(γ, n)^{196g}Au monitor reaction. The observed number of counts ($N_{obs}^{E_e}$) for the 355.68 keV γ-line of ^{196g}Au was calculated by summing the counts under the full energy peak and subtracting the linear Compton back-ground, which is related to the integrated photon flux $\Phi(E_e)$ as follows [24]:

$$\Phi(E_e)=\frac{N_{obs}^{E_e}(CL/LT)\lambda}{n\langle\sigma_R(E_e)\rangle I_\gamma\varepsilon_\gamma(1-e^{-\lambda T_{irr}})e^{-\lambda T_c}(1-e^{-\lambda CL})}, \quad (1)$$

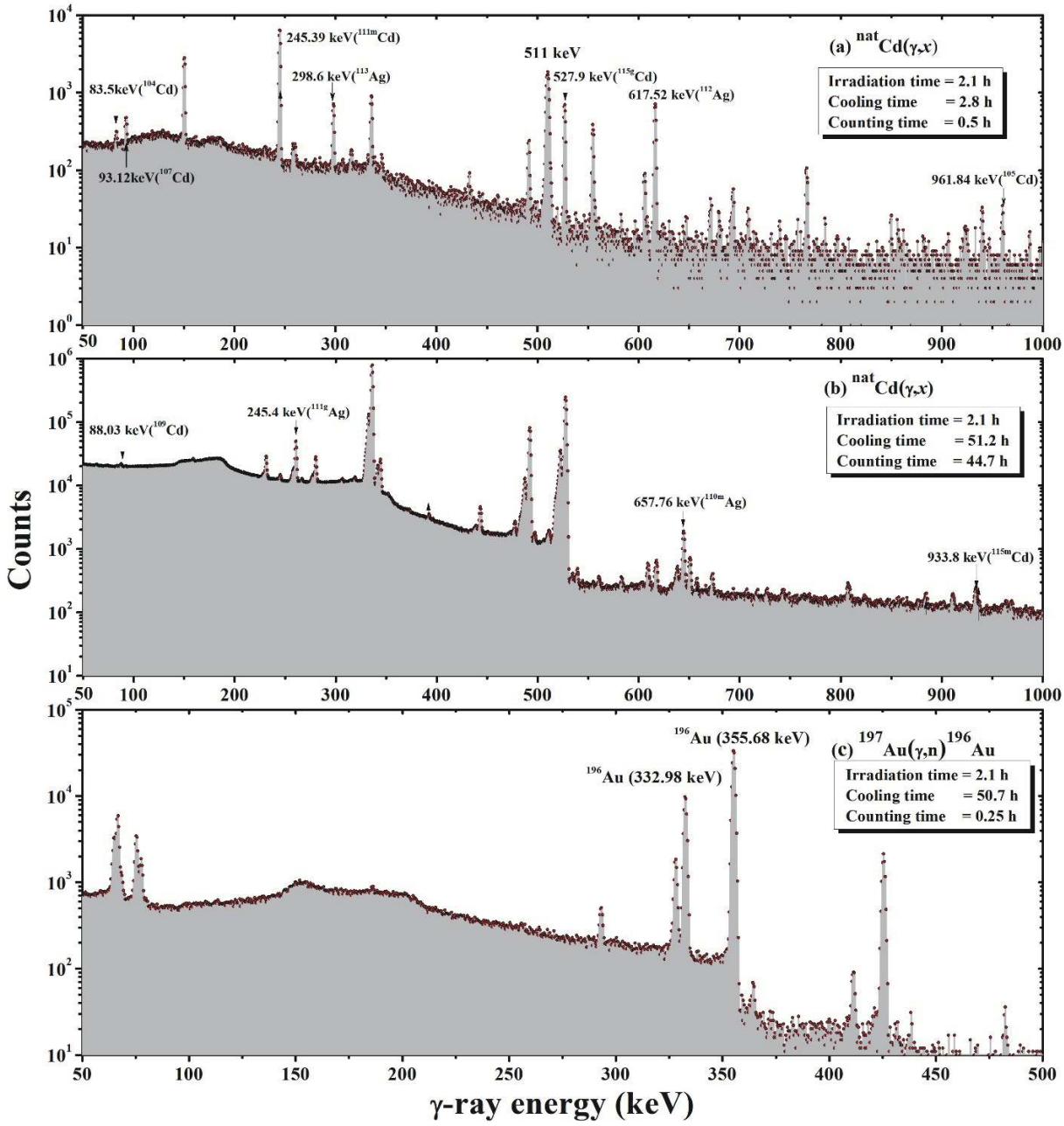

Fig. 1. (color online) Typical γ-ray spectra of the products of the ^{nat}Cd(γ, x) reactions with cooling times of (a) 2.8 h and (b) 51.2 h, and (c) those of the ^{197}Au(g, n) reaction with a cooling time of 50.7 h. The bremsstrahlung end-point energy used for the irradiation was 60 MeV.

where n and λ are the number of atoms in the flux monitor (Au) sample and the decay constant for ^{196g}Au, respectively. I_γ and ε_γ are the branching intensity and detection efficiency of the selected γ-line, respectively. T_{irr} and T_C, are the irradiation and the cooling times, respectively. CL and LT are the clock and live counting times, respectively. The detection efficiencies were measured using the standard calibration sources of ^{152}Eu and ^{133}Ba. $\langle\sigma_R(E_e)\rangle$ is the known average cross section of the ^{197}Au(γ,n)^{196g}Au monitor reaction taken from Ref. [24], which is 103.3±12.1 mb and 102.4±9.5 mb for the bremsstrahlung end-point energies of 50 and 60 MeV, respectively. Nuclear data, such as the half-lives, γ-ray abundances, reaction Q-values, and threshold energies of the products, are given in Table 1 [21, 22].

B. Calculation of normalized yield and correction factor

Natural cadmium has eight stable isotopes with different isotopic abundances. The yield of the produced radio-

Table 1. Nuclear spectroscopic data of the products of the ^{nat}Cd(γ, *xn*), ^{nat}Cd(γ, *pxn*), and ^{197}Au(γ, *n*) reactions. The photo-peak activities of γ-ray energies marked with bold letters were used for calculations.

Nuclides (spin & parity)	Half-life	Decay mode (%)	g-ray energy /keV	γ-ray abundance (%)	Reactions	*Q*-value /MeV	Threshold /MeV
^{115g}Cd $(1/2)^+$	53.46 h	β^- : 100.00	336.24	45.9	^{116}Cd(γ, *n*) Decay of ^{115m}Ag ($T_{1/2}$ = 18 s) by β^-(79%)	−8.699	8.700
			527.90	**27.45**	Decay of ^{115g}Ag ($T_{1/2}$ = 20 m) by β^-(100%)		
^{115m}Cd $(11/2)^-$	44.56 d	β^-: 100.00	158.03	0.02	^{116}Cd(γ, *n*)	−8.699	8.700
			484.47	0.29	Decay of ^{115}Ag ($T_{1/2}$ = 20 m) by β^-(100%)		
			933.80	**2**			
^{111m}Cd $(11/2)^-$	48.5 m	IT : 100	150.82	29.1	^{111}Cd(γ, *g*')	0.0	0.0
					^{112}Cd(γ, *n*)	−9.394	9.394
					^{113}Cd(γ, 2*n*)	−15.934	15.935
					^{114}Cd(γ, 3*n*)	−24.977	24.980
			245.39	**94**	^{116}Cd(γ, 5*n*)	−39.817	39.824
^{109}Cd $(5/2)^+$	461.9 d	EC: 100	**88.03**	**3.64**	^{110}Cd(γ, *n*)	−9.915	9.915
					^{111}Cd(γ, 2*n*)	−16.891	16.892
					^{112}Cd(γ, 3*n*)	−26.285	26.288
					^{113}Cd(γ, 4*n*)	−32.824	32.829
					^{114}Cd(γ, 5*n*)	−41.867	41.875
					^{116}Cd(γ,7*n*)	−56.707	56.722
^{107}Cd $(5/2)^+$	6.5 h	EC :100	**93.12**	**4.7**	^{108}Cd(γ, *n*)	−10.334	10.334
					^{110}Cd(γ, 3*n*)	−27.572	27.575
					^{111}Cd(γ, 4*n*)	−34.547	34.553
					^{112}Cd(γ, 5*n*)	−43.941	43.950
					^{113}Cd(γ, 6*n*)	−50.481	50.493
			828.93	0.163	^{114}Cd(γ, 7*n*)	−59.524	59.541
					^{116}Cd(γ, 9*n*)	−74.364	74.390
^{105}Cd $(5/2)^+$	55.5 m	EC :100	346.87	4.2	^{106}Cd(γ, *n*)	−10.870	10.870
					^{108}Cd(γ, 3*n*)	−29.133	29.137
			433.24	2.81	^{110}Cd(γ, 5*n*)	−46.371	46.381
					^{111}Cd(γ, 6*n*)	−53.346	53.360
					^{112}Cd(γ, 7*n*)	−62.740	62.759
			961.84	**4.7**	^{113}Cd(γ, 8*n*)	−69.280	69.303
^{104}Cd $(0)^+$	57.7 m	EC :100	66.6	2.4	^{106}Cd(γ, 2*n*)	−19.306	19.308
					^{108}Cd(γ, 4*n*)	−37.569	37.576
			83.5	**47**	^{110}Cd(γ, 6*n*)	−54.808	54.822
			709.3	19.5	^{111}Cd(γ, 7*n*)	−61.783	61.802
					^{112}Cd(γ, 8*n*)	−71.177	71.201
^{113g}Ag $(1/2)^-$	5.37 h	β^- : 100.00	258.72	1.64	^{114}Cd(γ, *p*)	−10.277	10.278
					^{116}Cd(γ, *p*2*n*)	−25.117	25.120
			298.6	**10**	Decay of ^{113m}Ag ($T_{1/2}$ = 62 s, spin=7/2$^+$) by IT(64%)		

Continued on next page

Table 1-continued from previous

Nuclides (spin & parity)	Half-life	Decay mode (%)	g-ray energy /keV	γ-ray abundance (%)	Reactions	*Q*-value /MeV	Threshold /MeV
^{112}Ag (2)$^-$	3.13 h	β$^-$: 100.00	606.82	3.1	^{113}Cd(γ, *p*)	−9.749	9.749
			617.52	**43**	^{114}Cd(γ, *pn*)	−18.792	18.793
			694.87	2.9	^{116}Cd(γ, *p*3*n*)	−33.632	33.637
^{111g}Ag (1/2)$^-$	7.45 d	β$^-$: 100.00	245.40	1.24	^{112}Cd(γ, *p*)	−9.648	9.649
					^{113}Cd(γ, *pn*)	−16.188	16.189
					^{114}Cd(γ, *p*2*n*)	−25.231	25.234
					^{116}Cd(γ, *p*4*n*)	−40.071	40.079
			342.13	**7**	Decay of ^{111m}Ag ($T_{1/2}$ = 1.08 m, spin=7/2+) by IT (99.3%)		
^{110m}Ag (6)$^+$	249.83 d	IT : 1.33	**657.76**	**95.61**	^{111}Cd(γ, *p*)	−9.084	9.084
					^{112}Cd(γ, *pn*)	−18.478	18.479
					^{113}Cd(γ, *p*2*n*)	−25.018	25.021
		β- : 98.67	884.67	75	^{114}Cd(γ, *p*3*n*)	−34.061	34.066
					^{116}Cd(γ, *p*5*n*)	−48.901	48.912
^{196g}Au (2)$^-$	6.18 d	EC : 92.8 β- : 7.2	**355.68**	**87.0**	^{197}Au(γ, *n*)	−8.072	8.073

nuclides is the sum of the isotope contributions based on their production threshold energies, as shown in Table 1. The eleven radio nuclides in Table 1 can be produced from ^{nat}Cd(γ, *x*)*j* reactions with different threshold values. The normalized yield contribution ($Y_{i,j}(E_e)$) for each reaction of ^{i}Cd(γ, *x*)*j* was obtained as follows [25]:

$$Y_{i,j}(E_e) = \frac{\int_{E_{th}}^{E_e} A_i\,\sigma_{i,j}(E_\gamma)\phi(E_\gamma)\mathrm{d}E_\gamma}{\sum_{k=1}^{8}\int_{E_{th}}^{E_e} A_k\,\sigma_{k,j}(E_\gamma)\phi(E_\gamma)\mathrm{d}E_\gamma}, \quad (2)$$

where *i* and *k* are eight stable isotopes (*i*, *k* = 106, 108, 110, 111, 112, 113, 114, 116) in ^{nat}Cd, and *j* is eleven produced isotopes (^{115g,m,111m,109,107,105,104}Cd and ^{113g,112,111g,110m}Ag). $\phi(E_\gamma)$ is the photon flux calculated using the GEANT4 code [23], $A_{i(k)}$ is the isotopic abundance, and $\sigma_{i,j}(E_\gamma)$ is the cross section for the ^{i}Cd(γ, *x*)*j* reactions at the photon energy E_γ, which was calculated using the TALYS 1.95 code [17]. The normalized yield contributions for eleven radio isotopes *j* produced from various ^{i}Cd(γ, *x*)*j* reactions are given in Table 2.

The threshold value (E_{th}) of the monitor reaction ^{197}Au(γ, *n*)^{196}Au is 8.07 MeV, as seen in Table 1. However, the production thresholds for the elevenradionuclides (*j* = $^{115g,m;111m;109m,107m;105m;104m}$Cd and $^{113g;112;111g;110m}$Ag) are different from the monitor reaction as listed in Table 1. Therefore, a flux correction factor is required to correct the measured photon flux from the ^{i}Cd(γ, *x*)*j* reactions to that from the monitor reaction. The photon flux correction factors $F_{i,j}(E_e)$ for ^{i}Cd(γ, *x*)*j* were calculated as follows [25]:

$$F_{i,j}(E_e) = \int_{E_{th}^{i,j}}^{E_e}\phi(E_\gamma)\mathrm{d}E_\gamma \Big/ \int_{E_{th}^{Au}}^{E_e}\phi(E_\gamma)\mathrm{d}E_\gamma, \quad (3)$$

where *i* and *j* have the same definitions as in Eq. (2). $E_{th}^{i,j}$ and E_{th}^{Au} are the threshold energies for the ^{i}Cd(γ, *x*)*j* and ^{197}Au(γ,*n*)^{196g}Au reactions, respectively. $\phi(E_\gamma)$ is the photon flux as a function of photon energy E_γ, taken from Fig. 2, which was simulated using the GEANT4 code [23]. The obtained correction factors to correct the different reactions to the monitor reaction are given in Table 2.

The yield-weighted flux correction factors $C_j^T(E_e)$ for the ^{j}Cd(γ, *x*)*j* reactions were calculated using Eqs. (2) and (3) as follows:

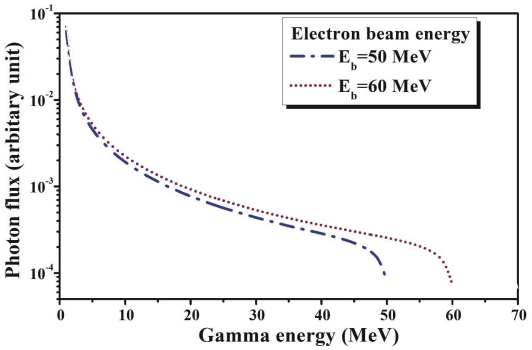

Fig. 2. (color online) Typical bremsstrahlung spectra for the end-point energies of 50 and 60 MeV simulated using the GEANT4 code.

Table 2. Normalized yield (%) and photon flux correction factor ($F_{i,j}(E_e)$) for the ^{i}Cd(γ, *xn*)*j* reactions.

Produced Nuclei	Reaction	E_{th}/MeV	E_e =50 MeV		E_e =60 MeV	
			$Y_{i,j}(E_e)$	$F_{i,j}(E_e)$	$Y_{i,j}(E_e)$	$F_{i,j}(E_e)$
^{115g}Cd	^{116}Cd(γ, *n*)	8.70	$Y_{116,115}$= 100	$F_{116,115}$= 0.934	$Y_{116,115}$ = 100	$F_{116,115}$= 0.940
^{115m}Cd	^{116}Cd(γ, *n*)	8.70	$Y_{116,115}$= 100	$F_{116,115}$= 0.934	$Y_{116,115}$ = 100	$F_{116,115}$= 0.940
^{111m}Cd	^{111}Cd(γ, *g*')	0.0	$Y_{111,111}$= 1.70	$F_{111,111}$= 2.910	$Y_{111,111}$ =1.40	$F_{111,111}$= 2.710
	^{112}Cd(γ, *n*)	9.39	$Y_{112,111}$= 64.9	$F_{112,111}$= 0.890	$Y_{112,111}$=62.6	$F_{112,111}$= 0.901
	^{113}Cd(γ, 2*n*)	15.94	$Y_{113,111}$= 18.5	$F_{113,111}$= 0.554	$Y_{113,111}$= 19.0	$F_{113,111}$= 0.592
	^{114}Cd(γ, 3*n*)	24.96	$Y_{114,111}$= 14.5	$F_{114,111}$= 0.306	$Y_{114,111}$= 16.0	$F_{114,111}$= 0.359
	^{116}Cd(γ, 5*n*)	39.82	$Y_{116,111}$= 0.40	$F_{116,111}$= 0.080	$Y_{116,111}$= 1.00	$F_{116,111}$= 0.148
^{109}Cd	^{110}Cd(γ, *n*)	9.92	$Y_{110,109}$= 75.7	$F_{110,109}$= 0.848	$Y_{110,109}$= 74.1	$F_{110,109}$= 0.863
	^{111}Cd(γ, 2*n*)	16.89	$Y_{111,109}$= 18.7	$F_{111,109}$= 0.518	$Y_{111,109}$= 18.7	$F_{111,109}$= 0.560
	^{112}Cd(γ, 3*n*)	26.29	$Y_{112,109}$= 4.60	$F_{112,109}$= 0.278	$Y_{112,109}$= 5.00	$F_{112,109}$= 0.333
	^{113}Cd(γ, 4*n*)	32.83	$Y_{113,109}$= 0.80	$F_{113,109}$= 0.168	$Y_{113,109}$= 1.10	$F_{113,109}$= 0.231
	^{114}Cd(γ, 5*n*)	41.86	$Y_{114,109}$= 0.20	$F_{114,109}$= 0.059	$Y_{114,109}$= 1.10	$F_{114,109}$= 0.127
^{107}Cd	^{108}Cd(γ, *n*)	10.33	$Y_{108,107}$= 67.5	$F_{108,107}$= 0.823	$Y_{108,107}$= 59.2	$F_{108,107}$= 0.840
	^{110}Cd(γ, 3*n*)	27.58	$Y_{110,107}$= 24.7	$F_{110,107}$= 0.255	$Y_{110,107}$= 24.5	$F_{110,107}$= 0.316
	^{111}Cd(γ, 4*n*)	34.55	$Y_{111,107}$= 7.30	$F_{111,107}$= 0.145	$Y_{111,107}$= 10.1	$F_{111,107}$= 0.210
	^{112}Cd(γ, 5*n*)	43.95	$Y_{112,107}$= 0.50	$F_{112,107}$= 0.039	$Y_{112,107}$= 5.80	$F_{112,107}$= 0.108
	^{113}Cd(γ, 6*n*)	50.49	$Y_{113,107}$= 0.00	$F_{113,107}$= 0.00	$Y_{113,107}$= 0.40	$F_{113,107}$= 0.052
^{105}Cd	^{106}Cd(γ, *n*)	10.87	$Y_{106,105}$= 98.6	$F_{106,105}$= 0.786	$Y_{106,105}$= 96.4	$F_{106,105}$= 0.806
	^{108}Cd(γ, 3*n*)	29.14	$Y_{108,105}$= 1.40	$F_{108,105}$= 0.227	$Y_{108,105}$= 1.60	$F_{108,105}$= 0.286
	^{110}Cd(γ, 5*n*)	46.38	$Y_{110,105}$= 0.00	$F_{110,105}$= 0.020	$Y_{110,105}$= 1.90	$F_{110,105}$= 0.086
	^{111}Cd(γ, 6*n*)	53.36	$Y_{111,105}$= 0.00	$F_{111,105}$= 0.000	$Y_{110,105}$= 0.10	$F_{111,105}$= 0.033
^{104}Cd	^{106}Cd(γ, 2*n*)	19.31	$Y_{106,104}$= 98.2	$F_{106,104}$= 0.443	$Y_{106,104}$= 96.2	$F_{106,104}$= 0.488
	^{108}Cd(γ, 4*n*)	37.58	$Y_{108,104}$= 1.80	$F_{108,104}$= 0.107	$Y_{108,104}$= 3.60	$F_{108,104}$= 0.174
	^{110}Cd(γ, 6*n*)	54.82	$Y_{110,104}$= 0.00	$F_{110,104}$= 0.000	$Y_{110,104}$= 0.20	$F_{110,104}$= 0.016
^{113}Ag	^{114}Cd(γ, *p*)	10.28	$Y_{114,113}$= 88.1	$F_{114,113}$= 0.823	$Y_{114,113}$= 92.9	$F_{114,113}$= 0.840
	^{116}Cd(γ, *p*2*n*)	25.12	$Y_{116,113}$= 11.9	$F_{116,113}$= 0.302	$Y_{116,113}$= 7.10	$F_{116,113}$= 0.356
^{112}Ag	^{113}Cd(γ, *p*)	9.75	$Y_{113,112}$= 27.0	$F_{113,112}$= 0.862	$Y_{113,112}$= 21.9	$F_{113,112}$= 0.875
	^{114}Cd(γ, *pn*)	18.79	$Y_{114,112}$= 71.8	$F_{114,112}$= 0.460	$Y_{114,112}$= 74.3	$F_{114,112}$= 0.505
	^{116}Cd(γ, *p*3*n*)	33.64	$Y_{116,112}$= 1.20	$F_{116,112}$= 0.156	$Y_{116,112}$= 3.80	$F_{116,112}$= 0.234
^{111}Ag	^{112}Cd(γ, *p*)	9.65	$Y_{112,111}$= 56.9	$F_{112,111}$= 0.862	$Y_{112,111}$= 49.9	$F_{112,111}$= 0.875
	^{113}Cd(γ, *pn*)	16.19	$Y_{113,111}$= 23.1	$F_{113,111}$= 0.546	$Y_{113,111}$= 23.0	$F_{113,111}$= 0.585
	^{114}Cd(γ, *p*2*n*)	25.23	$Y_{114,111}$= 19.9	$F_{114,111}$= 0.297	$Y_{114,111}$= 26.5	$F_{114,111}$= 0.352
	^{116}Cd(γ, *p*4*n*)	40.08	$Y_{116,111}$= 0.10	$F_{116,111}$= 0.078	$Y_{116,111}$= 0.60	$F_{116,111}$= 0.146
^{110m}Ag	^{111}Cd(γ, *p*)	9.08	$Y_{111,110}$= 17.5	$F_{111,110}$= 0.905	$Y_{111,110}$= 10.7	$F_{111,110}$= 0.914
	^{112}Cd(γ, *pn*)	18.48	$Y_{112,110}$= 58.7	$F_{112,110}$= 0.466	$Y_{112,110}$= 49.2	$F_{112,110}$= 0.511
	^{113}Cd(γ, *p*2*n*)	25.02	$Y_{113,110}$= 16.4	$F_{113,110}$= 0.301	$Y_{113,110}$= 18.3	$F_{113,110}$= 0.356
	^{114}Cd(γ, *p*3*n*)	34.06	$Y_{114,110}$= 7.40	$F_{114,110}$= 0.151	$Y_{114,110}$= 21.6	$F_{114,110}$= 0.215
	^{116}Cd(γ, *p*5*n*)	48.91	$Y_{116,110}$= 0.00	$F_{116,110}$= 0.004	$Y_{116,110}$= 0.20	$F_{116,110}$= 0.065

$$C_j^T(E_e) = \sum_i \left(Y_{i,j}(E_e) \times F_{i,j}(E_e)\right) \Big/ \sum_i Y_{i,j}(E_e). \quad (4)$$

The obtained yield-weighted flux correction factors $C_j^T(E_e)$ for the eleven produced isotopes (j) are listed in Table 3. The yield-weighted photon flux $\Phi_j^C(E_e)$ with the yield-weighted flux correction factors for the ^{nat}Cd(γ, x)j reactions were obtained as follows:

$$\Phi_j^C(E_e) = C_j^T(E_e) \times \Phi(E_e). \quad (5)$$

C. Measurement of flux-weighted average cross sections

We determined the flux-weighted average cross sections using the yield-weighted photon flux $\Phi_j^C(E_e)$ for the ^{nat}Cd(γ, x)j reactions (the produced nuclei j is given as ^{115gm,111m,109,107,105,104}Cd and ^{113g,112,111g,110m}Ag). The nuclear spectroscopic data for the reaction products were taken from Refs. [21, 22] and given in Table 1. Once the observed number counts under the photo-peak ($N_{obs}^{E_\gamma}$) was acquired for the characteristic γ-ray energy of the produced radionuclide j, the flux-weighted average cross sections of the ^{nat}Cd(γ, x)j reactions were obtained as follows [25]:

$$\left\langle \sigma_j^{nat}(E_e) \right\rangle = \frac{N_{obs}^{E_e}(CL/LT)\lambda}{n\Phi_j^C(E_e) I_\gamma \varepsilon_\gamma (1-e^{-\lambda T_{irr}}) e^{-\lambda T_c}(1-e^{-\lambda CL})}, \quad (6)$$

where all terms have the same meaning as in Eq. (1) and $\Phi_j^C(E_e)$ is the yield-weighted photon flux as given in Eq. (5).

D. Theoretical calculations of flux-weighted average cross sections

The flux-weighted average cross sections were also theoretically calculated for all the residual nuclides of interest based on the TALYS 1.95 [17] and EMPIRE-3.2 Malta [18] nuclear codes and compared with the experimental data, which are presented in Table 4. The calculations based on TALYS 1.95 [17] and EMPIRE-3.2 Malta [18] were performed with their default parameters. The photon-induced reaction cross sections ($\sigma_R^x(E_i)$) for the ^{nat}Cd(γ, x) reactions were calculated based on mono-energetic photons using the TALYS 1.95 [17] and EMPIRE-3.2 Malta [18] codes. In the calculations, all possible exit channels of the nuclear reactions of the given projectile energy were considered. The flux-weighted average cross sections ($\langle\sigma_x(E)\rangle$) for the ^{nat}Cd(γ, x) reactions were calculated as follows:

Table 3. Yield-weighted flux correction factor for the ^{nat}Cd(γ, x)j reactions.

Nuclear reactions	Total correction factors ($C_j^T(E_e)$)	
	Bremsstrahlung end-point energy, E_e/MeV	
	50	60
^{nat}Cd(γ, n)^{115g}Cd	0.934	0.941
^{nat}Cd(γ, n)^{115m}Cd	0.934	0.941
^{nat}Cd(γ, xn)^{111m}Cd	0.774	0.774
^{nat}Cd(γ, xn)^{109}Cd	0.753	0.765
^{nat}Cd(γ, xn)^{107}Cd	0.629	0.602
^{nat}Cd(γ, xn)^{105}Cd	0.778	0.783
^{nat}Cd(γ, xn)^{104}Cd	0.437	0.476
^{nat}Cd(γ, pxn)^{113g}Ag	0.761	0.806
^{nat}Cd(γ, pxn)^{112}Ag	0.565	0.576
^{nat}Cd(γ, pxn)^{111g}Ag	0.676	0.665
^{nat}Cd(γ, pxn)^{110m}Ag	0.492	0.416

$$\langle\sigma_x(E)\rangle = \int_{E_{th}}^{E_{\gamma max}} \sigma_R^x(E_i)\,\varphi(E_i)\mathrm{d}E \Big/ \int_{E_{th}}^{E_{\gamma max}} \varphi(E_i)\mathrm{d}E, \quad (7)$$

where (E_i) is the bremsstrahlung photon flux as a function of energy (E) simulated by the GEANT 4 code [23], as shown in Fig. 2.

IV. RESULTS AND DISCUSSION

The measured flux-weighted average cross sections are presented in different figures along with theoretical calculations and previously published data. The numerical values of all the cross sections and the uncertainties are given in Table 4. As previously stated, natural cadmium has eight stable isotopes (^{116,114,113,112,111,110,108,106}Cd). Thus, during irradiation, the production of a specific radionuclide is prone to contribution from many reaction channels based on the projectile energy.

The overall uncertainties in the results were calculated by taking the square root of the quadratic sum of all independent statistical and systematic uncertainties [19]. The resulting statistical uncertainties were mainly contributed by the counting statistics from the observed number of counts under the photo-peak of each γ-line (1.5%~10.5%). This was estimated by accumulating the data for an optimum time that depends on the half-life of the produced nuclides. In contrast, the systematic uncertainties were calculated from the uncertainties of the flux estimation (~11.5%), the detector efficiency (~3%), the half-life of the reaction products (~2%), the distance between the sample and detector (~2%), the γ-ray abundance (~2%), the irradiation and cooling time (~2%), the

Table 4. Flux-weighted average cross sections for the ^{nat}Cd(γ, *xn*) and ^{nat}Cd(γ, *pxn*) reactions.

Reaction	Bremsstrahlung end-point energy/MeV	Flux-weighted average cross-section $\langle\sigma_i\rangle$/mb		
		Present work	Theoretical calculations	
			TALYS 1.95 [17]	Empire 3.2 Malta [18]
^{nat}Cd(γ, *xn*)^{115g}Cd	50	2.432 ± 0.345	2.521	3.631
	60	2.123 ± 0.261	2.330	3.544
^{nat}Cd(γ, *xn*)^{115m}Cd	50	0.5 ± 0.071	0.534	0.778
	60	0.446 ± 0.059	0.493	0.760
^{nat}Cd(γ, *xn*)^{111m}Cd	50	1.461 ± 0.219	0.458	0.811
	60	1.413 ± 0.212	0.449	0.785
^{nat}Cd(γ, *xn*)^{109}Cd	50	12.346 ± 1.786	9.082	8.381
	60	10.210 ± 1.501	8.466	7.724
^{nat}Cd(γ, *xn*)^{107}Cd	50	0.733 ± 0.101	0.788	0.656
	60	0.681 ± 0.094	0.834	0.711
^{nat}Cd(γ, *xn*)^{105}Cd	50	0.43 ± 0.065	0.669	0.702
	60	0.385 ± 0.059	0.632	0.651
^{nat}Cd(γ, *xn*)^{104}Cd	50	0.105 ± 0.015	0.121	0.112
	60	0.087 ± 0.011	0.112	0.086
^{nat}Cd(γ, *xn*)$^{113g+m}$Ag	50	0.534 ± 0.075	0.057	0.108
	60	0.501 ± 0.061	0.057	0.110
^{nat}Cd(γ, *xn*)^{112}Ag	50	0.318 ± 0.043	0.068	0.159
	60	0.367 ± 0.046	0.081	0.172
^{nat}Cd(γ, *xn*)$^{111g+m}$Ag	50	0.126 ± 0.019	0.0425	0.121
	60	0.123 ± 0.018	0.045	0.119
^{nat}Cd(γ, *xn*)^{110m}Ag	50	0.026 ± 0.005	0.017	0.032
	60	0.027 ± 0.004	0.026	0.035

current and electron beam energy (~1%), and the number of cadmium target nuclei (~0.3%). The total systematic uncertainty is approximately 12.58%. The overall uncertainty is found to be between ~12.67% and ~16.07%.

A. Measured photo-nuclear reaction cross sections of cadmium isotopes

When natural cadmium is irradiated with bremsstrahlung radiation with end-point energies of 50 and 60 MeV, six cadmium isotopes are directly produced through ^{nat}Cd(γ, *xn*) reactions, except the ^{115g,m}Cd nuclides, which can be indirectly produced from the β$^-$ decay of ^{115g,m}Ag, as given in Table 1.

In this study, the flux-weighted average cross sections of the ^{nat}Cd(γ, *xn*)^{115g,m,111m,109,107,105,104}Cd reactions at the bremsstrahlung end-point energies of 50 MeV and 60 MeV are determined for the first time and presented in Table 4. All measurements of the produced cross sections of the cadmium isotopes are exclusive, that is, there is no contribution from any other short-lived radionuclides in the measurements. Even the ^{109,107,105,104}Cd radionuclides have no isomers; hence, their reaction cross sections are also independent. For comparison, the cross sections for the reactions as a function of the mono-energetic photons were calculated using the TALYS-1.95 and Empire 3.2 codes with default parameters; the flux-weighted average cross sections were then calculated using Eq. (7).

1. ^{nat}Cd(γ, n)$^{115g, 115m}$Cd reaction

The radioisotope ^{115}Cd is produced directly through the ^{116}Cd(γ, *n*) reaction and indirectly through the β$^-$ decay of ^{115}Ag. It has a short-lived ground state ^{115g}Cd ($T_{1/2}$=53.46 h) and a long-lived meta-stable state ^{115m}Cd ($T_{1/2}$=44.56 d). The simplified energy level and the decay scheme of ^{115m,g}Cd is shown in Fig. 3. The meta-stable state ^{115m}Cd with a half-life of 44.6 d decays directly to the ground state of ^{115}In by the β$^-$ process with a branching ratio of 97%. Meanwhile, approximately 1.7% of the

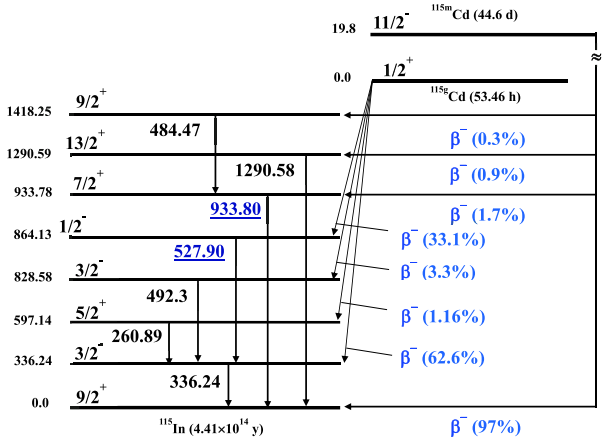

Fig. 3. (color online) Simplified decay scheme of the ^{115g,,m}Cd isomers.

meta-stable state decays to the ground state of ^{115}In (j^{π}=9/2^{+}) through the excited state of ^{115}In (j^{π}=7/2^{+}) by emitting a 933.8 keV γ-ray. The unstable ground state ^{115g}Cd (j^{π}=1/2^{+}) decays to the 336.24 keV state of ^{115}In (J^{π} = 1/2^{-}) by a β^{-} process with a branching ratio of 62.6%, which decays to the ground state of ^{115}In (J^{π} = 9/2^{+}) via M4 transition by emitting a characteristic γ-ray of 336.2 keV. On the other hand, the unstable ground state ^{115g}Cd decays to the 864.1 keV state of ^{115}In (J^{π} = 1/2^{+}) by a β^{-} process with a branching ratio of 33.1%, which then decays to the 336.2 keV state of ^{115}In (J^{π} = 1/2^{-}) by emitting a 527.9-keV γ-ray. In order to identify the ^{115m,g}Cd isomeric pairs, we used the 933.8 keV and 527.9 keV photo-peaks for the ^{115m}Cd and ^{115g}Cd nuclides, respectively. It is observed that both the metastable and ground states seem to be individual.

The measured results for the ^{nat}Cd(γ, *xn*)$^{115g;115m}$Cd reactions are compared with the theoretical values obtained with the TALYS-1.95 and Empire 3.2 codes, as shown in Fig. 4. There is no literature data for the ^{nat}Cd(γ, *xn*)^{115g}Cd reaction. It is clear that the theoretical values from both the TALYS-1.95 and Empire 3.2 codes are in agreement with the data from this study, as shown in Fig. 4. However, there is only one set of literature data regarding the low energy side of the GDR region for the ^{nat}Cd(γ, *xn*)^{115m}Cd reaction [8], which was obtained with monoenergetic photons. To compare those results with the results of this study, we calculated the flux-weighted average cross section for the literature value using Eq. (7), as shown in Fig. 4. The flux-weighted average cross sections for literature data in the low energy region were higher than the theoretical results. However, the present results are lower than the values obtained with the TALYS-1.95 and Empire 3.2 codes, as shown in Fig. 4.

Based on the measured experimental cross sections of the metastable and ground states from Table 4, we obtained the isomeric yield ratio (IR=σ_h/σ_l) of ^{115g}Cd (nuclear spin=1/2^{+}) and ^{115m}Cd (nuclear spin=11/2^{-}) in the ^{nat}Cd(γ, *xn*) reactions, which are given in Table 5 for various bremsstrahlung end-point energies. The photon-induced IR values from this study, the literature data in the GDR region [11-14], and our previous results [15] are listed in Table 5 and shown in Fig. 5. The IR values for neutron-induced ^{116}Cd(*n*, 2*n*)^{115g,m}Cd reactions taken from previous data [16] and those theoretically calculated using TALYS-1.95, EMPIRE-3.2 Malta, and TENDL-2019 [26] are also presented in Table 5 and Fig. 5.

In order to understand the effects of spin and input angular momentum, outgoing particles, and excitation energy, the IR values from the different reaction channels were compared. The average excitation energy ($\langle E^{*}(E)\rangle$) of the compound nucleus from the threshold energy (E_{th}) to the bremsstrahlung end-point energy (E_e) was determined using the following expression [27, 28]:

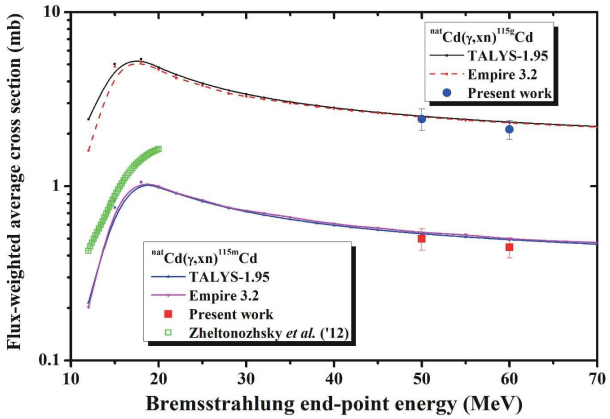

Fig. 4. (color online) The experimental flux-weighted average cross sections of ^{nat}Cd(γ, *xn*)^{115g}Cd and ^{nat}Cd(γ, *xn*)^{115m}Cd reactions as a function of bremsstrahlung end-point energy along with the theoretical calculations using the TALYS-1.95 and EMPIRE-3.2 codes.

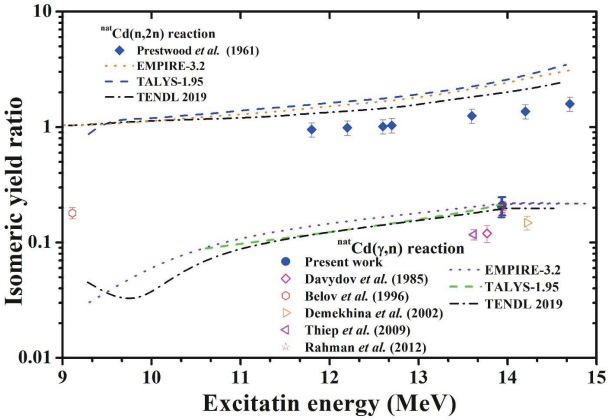

Fig. 5. (color online) Isomeric cross section ratio (IR=σ_h/σ_l) of ^{115g,m}Cd in the (γ, *n*) and (*n*, 2*n*) reactions as a function of excitation energy of the compound nucleus.

Table 5. Isomeric yield ratio of ^{115m,g}Cd from the ^{116}Cd(γ, *n*) and ^{116}Cd(*n*, 2*n*) reactions.

Reaction	Projectile energy/MeV	Excitation energy/MeV	Isomeric ratio ($IR = \sigma_{HighSpin}/\sigma_{LowSpin}$)		
			Experimental work [Ref.]	Theoretical calculations	
				TALYS 1.95 [17]	Empire 3.2 Malta [18]
^{nat}Cd(γ, *xn*)^{115g,m}Cd	50	13.922	**0.206 ± 0.041** [A]	0.212	0.214
	60	13.928	**0.210 ± 0.038** [A]	0.212	0.214
^{116}Cd(γ, *n*)^{115gm}Cd	9.43	9.072	0.180 ± 0.019 [12]	0.015	0.004
^{116}Cd(γ, *n*)^{115g,m}Cd	20	13.803	0.117 ± 0.012 [14]	0.205	0.213
^{116}Cd(γ, *n*)^{115g,m}Cd	20	13.803	0.148 ± 0.020 [11]	0.205	0.214
^{116}Cd(γ, *n*)^{115g,m}Cd	22	13.841	0.120 ± 0.020 [13]	0.209	0.214
^{116}Cd(γ, *n*)^{115g,m}Cd	23.5	13.857	0.158 ± 0.016 [14]	0.209	0.214
^{116}Cd(γ, *n*)^{115g,m}Cd	50	13.922	0.186 ± 0.020 [15]	0.212	0.214
^{116}Cd(γ, *n*)^{115g,m}Cd	60	13.928	0.202 ± 0.020 [15]	0.212	0.214
^{116}Cd(γ, *n*)^{115g,m}Cd	70	13.933	0.209 ± 0.019 [15]	0.212	0.214
^{116}Cd(*n*, 2*n*)^{115g,m}Cd	13.4	19.04	0.95 ± 0.13 [16]	1.321	1.189
^{116}Cd(*n*, 2*n*)^{115g,m}Cd	14	19.64	0.98 ± 0.14 [16]	1.360	1.246
^{116}Cd(*n*, 2*n*)^{115g,m}Cd	14.68	20.32	1.0 ± 0.14 [16]	1.398	1.295
^{116}Cd(*n*, 2*n*)^{115g,m}Cd	14.81	20.45	1.05 ± 0.15 [16]	1.410	1.295
^{116}Cd(*n*, 2*n*)^{115g,m}Cd	16.5	22.14	1.25 ± 0.18 [16]	1.510	1.364
^{116}Cd(*n*, 2*n*)^{115g,m}Cd	17.95	23.59	1.36 ± 0.19 [16]	2.810	2.690
^{116}Cd(*n*, 2*n*)^{115g,m}Cd	19.76	25.40	1.59 ± 0.22 [16]	3.461	3.101

[A] Present work.

$$\langle E^*(E_e)\rangle = \frac{\int_{E_{th}}^{E_e}\phi(E)\sigma_R(E)E\mathrm{d}E}{\int_{E_{th}}^{E_e}\phi(E)\sigma_R(E)\mathrm{d}E}, \quad (8)$$

where $\phi(E)$ represents the photon flux as a function of photon energy (E) for the bremsstrahlung spectra, which was calculated using the Geant4 code, as shown in the Fig. 2. The reaction cross section ($\sigma_R(E)$) was calculated using the default option in the TALYS-1.95 code. The calculated average excitation energies for the ^{116}Cd(γ,*n*) reaction corresponding to different bremsstrahlung end-point energies are given in Table 5.

The excitation energy (E^*) of the compound nucleus in the neutron and charged particle induced reactions was calculated as follows:

$$E^* = E_p + \left(\Delta_T + \Delta_p\right) - \Delta_{CN}, \quad (9)$$

where E_p is the projectile energy, and Δ_{CN}, Δ_T, and Δ_p are the mass excess values of the compound nucleus, target, and projectile, respectively. The mass excess values are taken from the Nuclear Wallet Cards [29].

As seen in Fig. 5, the experimental IR values in the ^{116}Cd(γ, *n*) reaction are in agreement with the theoretical values. However, in the ^{116}Cd(*n*, 2*n*) reaction, the theoretical values from TALYS-1.95, EMPIRE-3.2, and TENDL-2019 are higher than the experimental values. Additionally, in the ^{116}Cd(*n*, 2*n*) reaction, the theoretical values from TALYS-1.95 and EMPIRE-3.2 are slightly different. TENDL-2019 data are lower than the TALYS-1.95 data but are close to the experimental data. These differences are due to the use of default parameters in the current calculations with TALYS-1.95. Furthermore, the figure shows that the IR values of ^{115m,g}Cd increase with increasing excitation energy. However, at the same excitation energy, the IR values of ^{115m,g}Cd in the ^{116}Cd(*n*, 2*n*) reaction are significantly higher than those in the ^{116}Cd(γ, *n*) reaction. In the ^{116}Cd(γ, *n*) reaction, the compound nucleus is ^{116}Cd*, which has a 0^+ spin. On the other hand, in the ^{116}Cd(*n*, 2*n*) reaction, the compound nucleus is ^{117}Cd*, which has a $11/2^-$ spin in the excited state and $½^+$ spin in the ground state. At a high excitation energy, the compound nucleus of ^{117}Cd* with a high spin value of $11/2^-$ will be favorable in the ^{116}Cd(*n*, 2*n*) reaction. Thus, the high spin isomeric product ^{115m}Cd with a spin state of $11/2^-$ will preferably be populated in the ^{116}Cd(*n*, 2*n*) reaction, which results in a high IR value. This observation indicates the role of the spin of a compound nucleus alongside excitation energy. A similar observation can be made from our previous studies on the isomer ratio of ^{106m,g}Ag and ^{104m,g}Ag from the ^{nat}Ag (γ, *xn*) [30] and ^{nat}Ag(*n*, *xn*) [28] reactions, which support our present observations.

2. $^{nat}Cd(\gamma, xn)^{111m}Cd$ reaction

The isomeric state ^{111m}Cd (48.5 min, 11/2$^+$) was identified by the pure and independent 245.39 keV γ-line. For the production of ^{111m}Cd from the ^{112}Cd target, only two previous experimental data sets in the GDR energy region based on mono-energetic photons were available [8, 9]; these were found to be higher than the theoretical values obtained using the TALYS-1.95 and EMPIRE-3.2 Malta codes as shown in Fig. 6 and provided in Table 4. The figure and table also show that the current results follow the graphical shape but are higher than the theoretical values; they are the closest to the values calculated using the Empire-3.2 code.

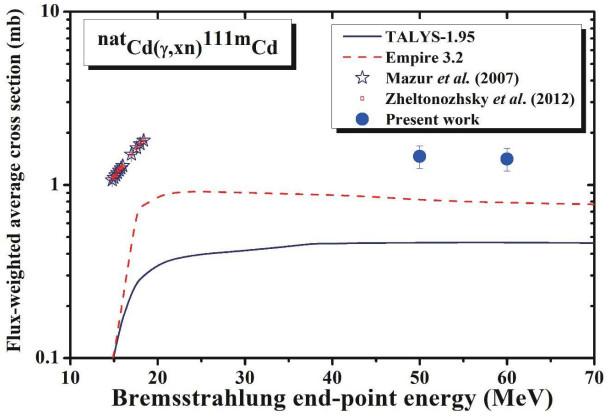

Fig. 6. (color online) Experimental flux-weighted average cross sections of the ^{nat}Cd(γ, *xn*)^{111m}Cd reaction as a function of bremsstrahlung end-point energy along with the theoretical calculations using the TALYS-1.95 and EMPIRE-3.2 codes.

3. $^{nat}Cd(\gamma, xn)^{109}Cd$ reaction

The radionuclide ^{109}Cd (461.9 d, 5/2$^+$) was identified by the pure and independent 88.03 keV γ-line. The measured ^{nat}Cd(γ, *xn*)^{109}Cd reaction cross-sections could onlybe compared with the theoretical calculations because no previous data has been found, as shown in Fig. 7 and tabulated in Table 4. In the figure, it is clear that the currently measured and theoretical values are in good agreement, in terms of not only shape but also magnitude.

4. $^{nat}Cd(\gamma, xn)^{107}Cd$ reactions

The flux-weighted average formation cross sections of ^{107}Cd (6.5 h, 5/2$^+$) were measured based on the 93.12 keV γ line. The measurements for the ^{nat}Cd(γ, *xn*)^{107}Cd reaction were performed for the first time and thus could only be compared with the theoretical values. Fig. 7 shows that the measurements are in good agreement with both of the calculations, but they are closer to the EMPIRE-3.2 Malta calculations.

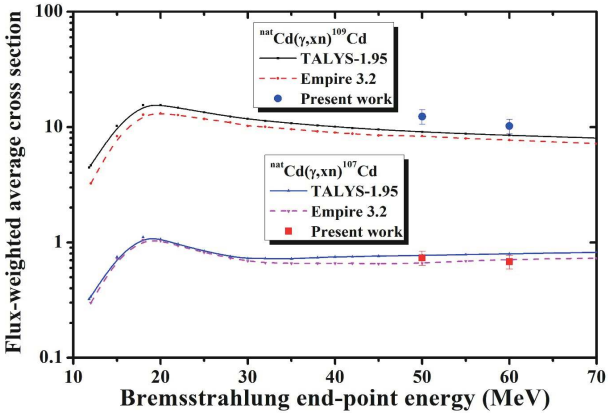

Fig. 7. (color online) Experimental flux-weighted average cross sections of the ^{nat}Cd(γ, *xn*)^{109}Cd and ^{nat}Cd(γ, *xn*)^{107}Cd reactions as a function of bremsstrahlung end-point energy along with the theoretical calculations using the TALYS-1.95 and EMPIRE-3.2 codes.

5. $^{nat}Cd(\gamma, xn)^{105}Cd$ reactions

The flux-weighted average formation cross sections for ^{105}Cd (55.5 min, 5/2$^+$) were measured based on the independent 961.84 keV γ-line. The radioisotope (^{105}Cd) is without an isomer. For this reaction, no literature data were available; hence, its measurements were also only compared with the theoretical calculations. In Fig. 8 and Table 4, it is clear that the flux-weighted average reaction cross sections calculated by the EMPIRE-3.2 Malta and TALYS-1.95 codes are almost the same, but they are higher than the currently presented results for the ^{nat}Cd(γ, *xn*)^{105}Cd reaction.

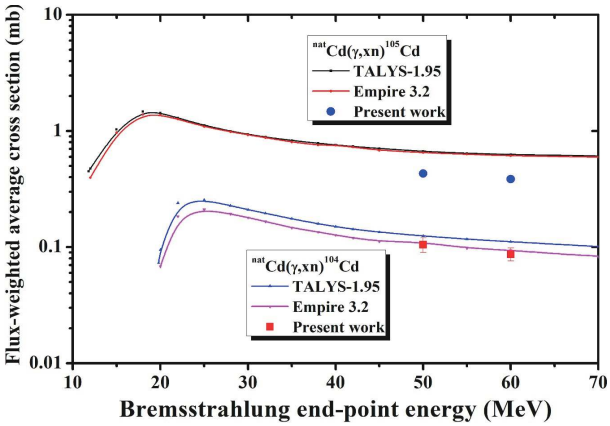

Fig. 8. (color online) Experimental flux-weighted average cross sections of the ^{nat}Cd(γ, *xn*)^{105}Cd and ^{nat}Cd(γ, *xn*)^{104}Cd reactions as a function of bremsstrahlung end-point energy along with the theoretical calculations using the TALYS-1.95 and EMPIRE-3.2 codes.

6. $^{nat}Cd(\gamma, xn)^{104}Cd$ reaction

The flux-weighted average formation cross section measurements of ^{104}Cd (57.7 min, 0^+) were also performed based onthe independent 83.5 keV γ-line. This reaction was studied for the first time and thus could only be compared with the theoretical values. In Table 4 and Fig. 8, the measured cross sections for the ^{nat}Cd(γ, *xn*)^{104}Cd reaction are shown to be in good agreement with both calculations in terms of shape and magnitude, but they are more precisely matched with the EMPIRE-3.2 Malta calculations.

B. Measured reaction cross-sections of silver radionuclides

Radioisotopes of silver (^{113g,112,111g,110m}Ag) were formed directly through (γ, *pxn*) reactions. During theirdirect production, ^{113g}Ag and ^{111g}Ag were populated by their short-lived metastable states by isomeric transition (IT). Therefore, their reaction cross sections were considered as cumulative values. ^{112}Ag has no isomer, while ^{110m}Ag has no contribution from any other radioisotope for its production; hence, their formation cross sections are exclusive and independent. Further details on silver residual nuclides are given below.

1. Cumulative $^{nat}Cd(\gamma, pxn)^{113g}Ag$ reaction

The deduced cumulative formation cross sections of ^{113g}Ag (5.37 h, $1/2^-$) include the direct production and the production through decay of the short-lived isomeric state ^{113m}Ag (62 s, $7/2^+$), as presented in Fig. 9 and listed in Table 4. Measurements of the ^{nat}Cd(γ, *pxn*)^{113g}Ag reaction cross sections were performed using the 298.6 keV γ-line. Moreover, it is important to note that the production probability of the meta-stable state is low due to its high spin state ($7/2^+$); therefore, we may conclude that ^{113m}Ag has a low contribution to the cumulative formation cross section of ^{113g}Ag. The measurements from the reaction were only compared with the theoretical values due to unavailability of published data. In Fig. 9(a), it is shown that the measured values for the reaction are higher than the calculated values; however, they exhibit the same tendency as the incident photon energy increases.

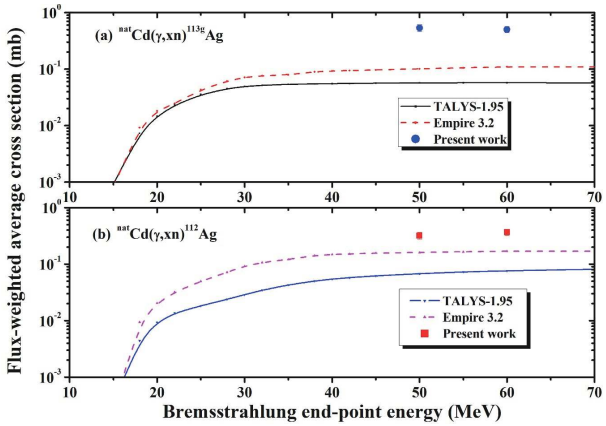

Fig. 9. (color online) Experimental flux-weighted average cross sections of the (a) ^{nat}Cd(γ, *x*)^{113g}Ag and (b) ^{nat}Cd(γ, *xn*)^{112}Ag reactions as a function of bremsstrahlung end-point energy along with the theoretical calculations using the TALYS-1.95 and EMPIRE-3.2 codes.

2. $^{nat}Cd(\gamma, pxn)^{112}Ag$ reaction

The ^{nat}Cd(γ, *pxn*)^{112}Ag reaction cross-sections were measured based on the 617.52 keV γ-line of ^{112}Ag (3.13 h, 2^-). This γ-line is also contributed to by ^{105}Cd and ^{106m}Ag. However, after separating the contributions, it was found that their combined contribution to the 617.52 keV γ-line was only ~2%-3%, and thus, they were added to the photo peak area uncertainty. These measurements were only compared with the theoretical values due to unavailability of published data. In Fig. 9(b) and Table 4, the measured values are revealed to be higher than the calculated values; however, both follow a similar trend when the incident photon energy is increased. Moreover, the magnitude of the current measurements are shown to be closer to the EMPIRE-3.2 calculation than the TALYS calculation.

3. Cumulative $^{nat}Cd(\gamma, pxn)^{111g}Ag$ reaction

For measurements of the flux-weighted average production cross section of ^{111g}Ag (7.45 d, $1/2^-$), the situation is the same as in the previous case with (^{113g}Ag). It is formed directly via the (γ, *pxn*) reaction and through the IT (99.3%) decay of the simultaneously produced short-lived ^{111m}Ag (1.08 min, $7/2^+$). In this case,the nuclear spin of the metastable state is higher; hence, its production probability is lower than that of the ground state. Based on this, we may once again conclude that the cumulative cross section measurements of ^{111g}Ag have a low ^{111m}Ag decay contribution. A comparison of the present results with theoretical values is shown in Fig. 10(a) and Table 4.

4. $^{nat}Cd(\gamma, pxn)^{110m}Ag$ reaction

Flux-weighted average production cross sections of ^{110m}Ag (249.83 d, 6^+) were measured based on the 657.76 keV γ-line. The gamma-ray spectrum was taken after sufficient time had passed to ensure other short-lived nuclides such as ^{105}Cd, which contaminate the 657.76 keV γ-line, had sufficiently decayed. The measured results, along with the calculated values, are shown in Fig. 10(b) and listed in Table 4. Both of the results are consistent and higher than the theoretical values but closer to the

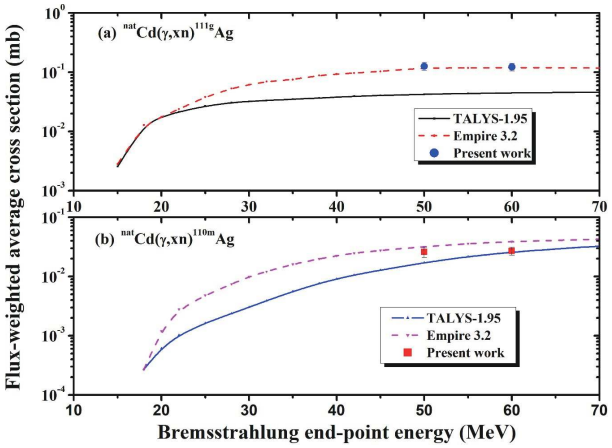

Fig. 10. (color online) Experimental flux-weighted average cross sections of the (a) ^{nat}Cd(γ, *xn*)^{111g}Ag and (b) ^{nat}Cd(γ, *xn*)^{110m}Ag reactions as a function of bremsstrahlung end-point energy along with the theoretical calculations using the TALYS-1.95 and EMPIRE-3.2 codes.

values calculated using the EMPIRE-3.2 code.

C. Integrated yield (Bq/g.μAh)

The production of cadmium and silver isotopes are important for medical and industrial applications and for a better understanding of their production in photon induced nuclear reactions. Therefore, the integrated yields (Bq/g.μAh) of cadmium and silver isotope productions from ^{nat}Cd(γ, *x*) reactions were measured in a procedure similar to that used for the integral yields of rhodium isotopes from the ^{103}Rh(γ, *x*) reaction [19, 31]. The integral yields of cadmium and silver isotope productions from ^{nat}Cd(γ, *x*) reactions are given in Table 6.

Table 6. Integral isotopic yield of different products from the ^{nat}Cd(γ, *xn*) and ^{nat}Cd(γ, *pxn*) reactions.

Reaction	Isotope	Yields/(Bq/g·A·h)	
		Bremsstrahlung end-point energy/MeV	
		50	60
^{nat}Cd(γ, *xn*)^{115g}Cd	^{115g}Cd	(8.83±0.57)×10^{6}	(8.52±0.60)×10^{7}
^{nat}Cd(γ, *xn*)^{115m}Cd	^{115m}Cd	(1.86±0.12)×10^{6}	(1.80±0.19)×10^{7}
^{nat}Cd(γ, *xn*)^{111m}Cd	^{111m}Cd	(4.48± 0.28)×10^{6}	(8.99±0.61)×10^{7}
^{nat}Cd(γ, *xn*)^{109}Cd	^{109}Cd	(3.62±0.26)×10^{7}	(2.49±0.21)×10^{8}
^{nat}Cd(γ, *xn*)^{107}Cd	^{107}Cd	(1.71±0.12)×10^{6}	(1.73± 0.12)×10^{7}
^{nat}Cd(γ, *xn*)^{105}Cd	^{105}Cd	(1.44±0.13)×10^{6}	(1.17±0.14)×10^{7}
^{nat}Cd(γ, *xn*)^{104}Cd	^{104}Cd	(1.8±0.12)×10^{5}	(1.73±0.15)×10^{6}
^{nat}Cd(γ, *pxn*)$^{113g+m}$Ag	$^{113m+g}$Ag	(1.58±0.11)×10^{6}	(1.67±0.11)×10^{7}
^{nat}Cd(γ, *pxn*)^{112}Ag	^{112}Ag	(7.0±0.41)×10^{5}	(8.74±0.53)×10^{6}
^{nat}Cd(γ, *pxn*)$^{111g+m}$Ag	^{111g}Ag	(3.3±0.24)×10^{5}	(3.55±0.32)×10^{6}
^{nat}Cd(γ, *pxn*)^{110m}Ag	^{110m}Ag	(6.0±0.65)×10^{4}	(5.6±0.40)×10^{5}

V. CONCLUSION

The flux-weighted average photon induced nuclear reaction cross-sections for the ^{nat}Cd(γ, *xn*; *x*=1-6) ^{115g,m,111m,109,107,105,104}Cd and ^{nat}Cd(γ, *xnyp*; *y*=1 *x*=1-5) ^{113g,112,111g,110m}Ag reactions as well as the isomeric yield ratios of ^{115g,m}Cd in the ^{116}Cd(γ, *n*) reaction were measured with the bremsstrahlung end-point energies of 50- and 60- MeV. Integral yield was also measured to assess the activities produced in the nuclear reactions. The photon induced formation reaction cross sections of ^{nat}Cd and the IR value of ^{115}Cd were calculated using the TALYS-1.95 and EMPIRE-3.2 codes and the evaluated data taken from the TENDL-2019 library. In most of the cases, calculated values from the TALYS and EMPIRE codes matched each other and the experimental value. It was also found that the flux-weighted average cross sections increased sharply in the GDR region due to photo absorption and then decreased slightly in QDR region due to the opening of particle emission reaction channels. The isomeric yield ratio of ^{115g,m}Cd in the ^{116}Cd(γ, *n*) reaction from this study and previously published data was compared with literature data for the ^{116}Cd(*n*, 2*n*) reaction. It was found that the experimental IR values of ^{115g,m}Cd in the ^{nat}Cd(γ, *xn*) reaction agree with the calculations but were well below the IR values due to the ^{116}Cd(*n*, 2*n*) reaction. The isomeric yield ratio previously measured in the ^{116}Cd(*n*, 2*n*) reaction was lower than the calculated values for the same reaction; this is most likely due to the use of default parameters in the theoretical calculations. It was also observed that the theoretical and experimental values increased with excitation energy. However, at the same excitation energy, the IR values in the ^{116}Cd(*n*, 2*n*) reaction were significantly higher than those in the ^{116}Cd(γ, *n*) reaction due to the higher spin of the compound nucleus in the former. This indicates the role of compound nucleus spin alongside the effect of excitation energy.

ACKNOWLEDGEMENT

The authors express their sincere thanks to the staff of the Pohang Accelerator Laboratory (PAL), Pohang, Korea, for the excellent operation and their support during the experiment.

References

[1] M. Berglund and M. E. Wieser, Pure Appl. Chem. **83**, 397 (2011)
[2] F. Tárkányi, B. Király, F. Ditrói *et al.*, Nucl. Instrum. Methods B **245**, 379 (2006)

[3] D. Filossofov, A. Novgorodov, N. Korolev *et al*., J. Appl. Radiat. Isot. **57**, 437 (2002)
[4] I. Hossain, N. Sharip, and K. Viswanathan, Sci. Res. Essays **7**, 86 (2012)
[5] J. Luo, F. Tuo, X. Kong *et al*., J. Appl. Radiat. Isot. **66**, 1920 (2008)
[6] A. Hermanne, S. Takács, F. Tárkányi *et al*., Nucl. Instrum. Methods B **217**, 193 (2004)
[7] S. M. Qaim, F. T. Tárkányi, P. Obložinský *et al*., J. Nucl. Sci. Tech. **39**, 1282 (2002)
[8] V. Zheltonozhskij, V. Mazur, D. Symochko *et al*., Yad. Fyizik. Energ. **44**, 140 (2012)
[9] V. Mazur, Z. Byigan, and D. Simochko, Ukrayins' kij Fyizichnij Zhurnal (Kyiv) **52**, 746 (2007)
[10] D. Kolev, E. Dobreva, N. Nenov *et al*., Nucl. Instrum. Methods A **356**, 390 (1995)
[11] N. Demekhina, A. Danagulyan, and G. Karapetyan, Phys. At. Nucl. **65**, 365 (2002)
[12] A. Belov, Y. P. Gangrsky, A. Tonchev *et al*., Phys. At. Nucl. **59**, 553 (1996)
[13] T. D. Thiep, T. T. An, N. T. Khai *et al*., Phys. Partic. Nucl. Lett. **6**, 126 (2009)
[14] M. Davydov, V. Magera, A. Trukhov *et al*., At. Energ. **58**, 47 (1985)
[15] M. S. Rahman, M. Lee, K.-S. Kim *et al*., Nucl. Instrum. Methods B **276**, 44 (2012)
[16] R. Prestwood and B. Bayhurst, Phys. Rev. **121**, 1438 (1961)
[17] A. Koning, S. Hilaire, and S. Goriely, TALYS-1.95. A Nuclear Reaction Program. A New Edition, December 2019
[18] M. Herman, R. Capote, M. Sin *et al*., *EMPIRE-3.2 Malta Modular system for nuclear reaction calculations*. 2013, Tech. Rep. INDC (NDS)-0642, BNL-101378-2013
[19] M. S. Rahman, K. Kim, G. Kim *et al*., Eur. Phys. J. A **52**, 194 (2016)
[20] V. D. Nguyen, D. K. Pham, T. T. Kim *et al*., J. Korean Phys. Soc. **50**, 417 (2007)
[21] R. B. Firestone and L. P. Ekstrom, Table of radioactive isotopes, version 2.1. 2004, Lawrence Berkeley National Laboratory. available at http://ie.lbl.gov/toi/index.asp
[22] *NuDat 2.6, National Nuclear Data Center, Brookhaven National Laboratory, updated 2011*; available at http://www.nndc.bnl.gov/
[23] S. Agostinelli, J. Allison, K. Amako *et al*., Nucl. Instrum. Methods A **506**, 250 (2003)
[24] H. Naik, G. Kim, K. Kim *et al*., Nucl. Phys. A **948**, 28 (2016)
[25] H. Naik, G. Kim, R. Schwengner *et al*., Eur. Phys. J. A **50**, 83 (2014)
[26] J. C. Sublet, A. Koning, D. Rochman *et al*., TENDL-2019: Delivering Both Completeness and Robustness, https://tendl.web.psi.ch/tendl_2019/tendl2019.html
[27] H. Thierens, D. De Frenne, E. Jacobs *et al*., Phys. Rev. C **14**, 1058 (1976)
[28] M. Nadeem, G. N. Kim, K. Kim *et al*., J. Radioanal. Nucl. Chem. **313**, 1 (2017)
[29] J. K. Tuli, Nuclear Wallet Cards, BNL, Upton, New York 11973-5000, USA.January 2000
[30] M. Tatari, G. N. Kim, H. Naik *et al*., J. Radioanal. Nucl. Chem. **300**, 269 (2014)
[31] J. P. François, R. Gijbels, and J. Hoste, J. Radioanal. Nucl. Chem. **5**, 251 (1970)